Received: 9 March 2023 | Revised: 6 August 2023 | Accepted: 4 September 2023

DOI: 10.1002/ese3.1572

ORIGINAL ARTICLE

An insight into a combined effect of backsheet and EVA encapsulant on field degradation of PV modules

Claudia Buerhop | **Tobias Pickel** | **Oleksandr Stroyuk** | **Jens Hauch** | **Ian Marius Peters**

High Throughput Methods in Photovoltaics, Forschungszentrum Jülich GmbH, Helmholtz Institute Erlangen-Nürnberg for Renewable Energy (HI ERN), Erlangen, Germany

Correspondence
Claudia Buerhop, High Throughput Methods in Photovoltaics, Forschungszentrum Jülich GmbH, Helmholtz Institute Erlangen-Nürnberg for Renewable Energy (HI ERN), Immerwahrstraße 2, 91058 Erlangen, Germany.
Email: c.buerhop-lutz@fz-juelich.de

Funding information
Zentrales Innovationprogramm Mittelstand; German Federal Ministry for Economic Affairs and Energy; The Bavarian State Government

Abstract

Polymer components, in particular, backsheets (BSs) and ethylene-vinyl acetate (EVA) encapsulants, play a crucial role in the degradation of commercial silicon photovoltaic (PV) modules. Degradation mechanisms depend in a complex way on the composition and properties of all involved polymers. In this study, we demonstrate that differences in the composition of EVA encapsulants, in particular, the presence of additives, such as UV blockers, affect the degradative processes in a decisive way, even for modules with identical BSs. A combination of spectral, imaging, and electrical characterization techniques applied in a mixed lab/field study showed that the field aging of PV modules with the same BSs and different encapsulant components results in the development of different degradation signs, such as insulation resistance loss, corrosion of metal interconnects, water ingress, oxidation depth in the encapsulant, and potential-induced degradation, depending on the presence of additives in the encapsulant. The present study provides an outlook on the complex influence of polymer components on the lifetime and performance of silicon PV modules.

KEYWORDS
energy systems, life cycle analysis, photovoltaics, solar energy

1 | INTRODUCTION

The performance and lifetime of silicon photovoltaic (PV) modules are recognized to be dependent on various intrinsic factors of chemical, technological, and engineering nature, as well as on extrinsic factors such as conditions of installation and maintenance.[1–3] These numerous factors can intertwine and produce unexpected effects, such as potential-induced degradation (PID),[1–3] or a relatively fast field degradation of polymer insulating components that are deemed highly stable based on lab tests.[2–6]

Recent studies of several groups, including some of the present authors, showed a considerable influence of the composition and structure of the polymer backsheet (BS) of PV modules on their lifetime, performance, electrical insulation, operational safety, and so forth.[1,3,6–8] In particular, we identified some clear BS-dependent trends in the development of corrosion and insulation resistance loss of PV modules, which

translated to issues on the string—and inverter level and resulted in late (no) starts of inverters, and in humidity-dependent performance losses.[7–10]

Along with BS materials, the composition and quality of transparent polymer encapsulants hosting the silicon cells have recently been recognized as a very important actor in the field degradation of PV modules.[2,4,5,11] Currently, the total majority of field-deployed silicon PV modules contain cross-linked ethylene-vinyl acetate (EVA) copolymer encapsulants showing a highly beneficial combination of relatively low cost, high light transmittance, good adhesion to glass, as well as relatively high stability toward UV illumination, and environmental factors, such as water permeation.[4,5] The stability and compatibility of EVA encapsulants can be further enhanced by various additives, including UV-light absorbers and stabilizers, antioxidants, adhesives, and so forth, typically introduced on the level of 0.1–0.3 wt%.[4,5]

A deeper insight into the origins and mechanisms of field degradation of BS materials revealed that this process is initiated by decomposition products of EVA copolymer encapsulant, formed either during module production or during field deployment and operation under the influence of solar irradiation.[4–6] In particular, acetic acid is formed during the obligatory procedure of thermally induced cross-linkage of the EVA encapsulant due to the partial elimination of acetate groups.[5,6,12] In addition, UV-light induces photochemical transformations of the EVA encapsulant even after cross-linkage, one of the main processes being the Norrish II type photoelimination, resulting in the formation of acetic acid and C=C double bonds in the EVA matrix.[5,6,12] These photochemical processes provide a second source of acetic acid in the PV modules.

Acetic acid produced in either way can adversely affect other module components, for example, by inducing corrosion of the metal interconnects or via degradation of BS layers due to acid-catalyzed fragmentation reactions.[6,13–15] It is evident that the scale of these events depends strongly on the capacity of EVA to produce acetic acid and on the diffusion of the acid within and out of the module, which in turn depends on the level of cross-linking and the presence of additives capable of reacting with acetic acid. Moreover, the presence of UV-blocking agents in EVA layers determines whether the solar UV light can penetrate through the EVA layer and induce photochemical degradation in the BS layers.

On the other side, penetration of environmental gases, in particular oxygen, and of moisture into PV modules through BSs can result in oxidative corrosion of metal interconnects and secondary oxidative degradation of polymer insulation, both processes accelerated by BS degradation.[6,11,16] It is evident that the composition and rheology of EVA layers, as well as the presence of additives, should strongly affect the probability and rate of these degradative processes. In summary, the quality of the polymer insulation, environmental resistance of PV modules, and, eventually, their lifetime are expected to be a complex function of the properties of both BS and EVA encapsulants, both of which can vary independently. As the bill of materials (BOM) of the PV modules is generally not disclosed, the analysis of possible BS/EVA combinations and their effect on the PV module performance turns out to be a major experimental challenge.

In the present paper, we provide an attempt to address this challenge by combining a lab-based study of a series of PV modules with different BS/EVA combinations with a field measurement campaign focused on a single specific BS type coupled with different EVAs. Based on our previous experience,[7–10,17,18] we explore the properties of PV modules by a combination of spectral methods (probing composition of BSs), UV-excited fluorescence (UVF) imaging (probing types of EVA), IR imaging (probing module performance), and insulation resistance measurements (probing general degradation state of a module).

We show that differences in the composition of the EVA encapsulants, in particular, the presence of specific additives, can affect the degradation pathways and patterns in a rather decisive way, even for the PV modules with identical BS materials. The EVA-dependent variation of the degradation behavior is observed in the development of insulation resistance losses, corrosion of interconnects, depth and pathways of degradation of BS and the encapsulant itself, development of the PID, and so forth.

2 | METHODS

2.1 | Lab measurements

UVF images were collected by illuminating modules with two MBJ Smart UV lamps (360–370 nm) and taking pictures in the dark with a camera operating in visible light with 2-s exposure.

The BS composition and stacking order of BS layers were identified by cross-sectional Raman microspectroscopy, as discussed in detail previously.[17] Raman spectroscopic measurements were performed on BS cross-section samples produced by detaching a piece of BS from a PV module and cutting the cross-section edge along the length of the BS. Raman spectra and spectral

maps were detected on a WITec alpha700 confocal Raman microscope in a spectral range of 130–3700 cm^{-1} and a resolution of 3 cm^{-1}. The samples were excited by a 532 nm laser with a maximal power of 7 mW. Spectral maps were constructed by scanning square (500 × 500 μm) sections of the sample with a resolution of 100 × 100 spectral points, yielding a spatial resolution of ca. 5 μm.

A database of cross-sectional maps was assembled and each map was associated with a near-infrared absorption (NIRA) spectrum taken from the air side of the corresponding cross-section. Using the database, NIRA spectroscopy can then be used as a self-standing nondestructive method for the identification of BS structure, as discussed in detail in Ref.[18]

NIR reflectance was measured with a fiber-coupled FT-NIR Rocket 2.6 spectrometer (Arcoptix) in a spectral range of 900–2600 nm (3800–11,000 cm^{-1}) with a resolution of 8 cm^{-1}. The samples were excited by a stabilized optical fiber-coupled NIR source SLS201/M (Thorlabs). The angle between the incident and the reflected light beam was 90°. The penetration depth of NIR light is on the order of 1 mm, allowing the entire BS (typical thickness of 300–600 μm) as well as the underlying EVA layer to be probed simultaneously.

The NIRA spectroscopy is insensitive to inorganic components of PV modules, allowing the frontal layer of EVA encapsulant to be probed with NIRA through the glass.[17] In a typical NIRA measurement of EVA encapsulant, a NIR reflectance (NIRR) spectrum of EVA was registered from the frontal side of a PV module over a metal interconnect using the latter as a mirror. Then, the NIRR spectrum was divided by a lamp emission spectrum, resulting in the NIRA spectrum.[17] Several (3–4) NIRA spectra of EVA were taken along the interconnect and averaged.

The samples of EVA for Raman spectroscopic characterization (ca. 10 per 10 mm) were cut from modules close to the spots where NIRA measurements were performed. Several (3–4) EVA samples were extracted from each inspected module and their Raman spectra were averaged for further analysis.

The isolation resistance R_{iso} of the modules was determined by a "wet" leakage resistance lab test by complete immersion of a module into a bath filled with aqueous electrolyte, as described in detail in various studies.[7,8]

2.2 | Field measurements

A PV power station with a capacity of 1 MWp (about 4000 PV modules) installed in Germany in 2013 was studied. During the field test, PV modules were characterized by IR imaging, UVF imaging, visual inspection for the signs of corrosion, and NIRA spectroscopy from the frontal and air (BS) sides.

IR imaging was performed using a DJI Zenmuse XT2 camera mounted on a DJI M210 drone from an altitude of about 15 m at almost clear-sky conditions, irradiance >600 W/m^2, and 20–25°C ambient. IR images were evaluated for ca. 20% of the modules. The same modules were inspected visually both from the frontal and from the air sides for signs of corrosion of metal interconnects and cracking/delamination of the BSs.

NIRA spectra of the BSs (from the air side) and EVA encapsulant (from the frontal side over metal interconnects) were collected pairwise for ca. 10% of the PV modules. UVF imaging was performed manually at nighttime similarly to the lab tests for ca. 20% of the modules.

3 | RESULTS AND DISCUSSION

3.1 | Lab-based characterization

3.1.1 | General structure of UVF images

The fluorescence imaging of EVA encapsulant is a powerful tool for the noncontact investigation of the degradation status of silicon cells and polymer components of commercial PV modules.[12] As one of the possible further development of this method, we have recently shown the feasibility of identifying several BS types by analyzing the geometry of the fluorescence patterns of EVA encapsulant.[19] We assumed that the primary photochemical degradation of EVA encapsulant results in the partial elimination of acetate groups and formation of C=C species emitting UVF and acetic acid as a by-product as shown by earlier reports.[12,20–22] The following degradation of BSs induced by the acetic acid accelerates the penetration of environmental gases (O_2 and moisture) into the module. This results in a partial oxidative quenching of EVA UVF and the formation of specific geometric UVF patterns characteristic for each particular BS.[12,20,23–25]

The origins of EVA fluorescence still remain a debated issue. Earlier works[20–22] postulated the UVF emission of EVA originating from conjugated polyenes and polyene/carbonyl species formed by the photo-induced EVA degradation as discussed above. Later, alternative mechanisms were suggested assuming the UVF emission coming from the products of degradation of UV-absorbing additives in EVA copolymer.[12]

By NIRA measurements performed on strongly field-aged historical PV modules with ca. 30 years of field

exposure in Germany, we found that the UVF emission of the EVA encapsulants can indeed be related to the presence of unsaturated functionalities, in particular, C=C bonds. The tested module showed bright UVF areas with strongly quenched edges and cracks (Figure 1A), providing opportunities to evaluate the content of saturated and unsaturated species in EVA with strongly different UVF intensities. The NIRA measurements were performed in the second-overtone range (900–1600 nm) using an Avantes NIRLine spectrometer with relatively long signal accumulation times (30–60 s), allowing weak EVA signals to be detected in the reflectance mode over strongly light-scattering Si wafers. A special focus was placed on the 1000–1300 nm range, where second overtones of C=C–H vibration at 1120–1130 nm and C–C–H vibration at 1220–1230 nm (Figure 1B) can be observed and used for the evaluation of the relative content of unsaturated C=C species. NIRA spectra (Figure 1B) detected in the spots of low (Spot 1 in Figure 1C), intermediate (Spot 2), and high UVF intensity (Spot 3) show a distinct increase of the relative intensity of the C=C–H band with an increase of the UVF intensity. Mapping of a cell section presented in Figure 1C by NIRA with a 5-mm step confirms the direct relationship between the intensity of the C=C–H signal ($R_{C=C}$) and the UVF intensity (Figure 1D).

By collecting a database of UVF images of a series of PV modules with different BS structures, the latter determined by cross-sectional Raman spectroscopy (please find details of this procedure reported in various studies[17,18]), we were able to discriminate several BS by the characteristic geometry of the UVF patterns.[19] We showed that the UVF-based identification of BSs can be supported and automated by multivariate analysis of UVF intensity profiles and potentially used as a tool for high-throughput BS analysis in the field.[19]

3.1.2 | Effect of EVA encapsulant on UVF patterns—The case of PET BSs

Apart from the effect of the BS composition, the geometry of UVF patterns can be expected to depend on the properties of the EVA encapsulant, in particular, on the carbonyl content and on the presence of additives, such as UV-protecting agents and stabilizers. Our present lab experiments supported the latter assumption and showed that many module samples with the same BS types reveal rather different UVF patterns depending on the characteristics of accompanying EVA layers. In this view, our study focuses on modules with the same BS composition but different geometry of UVF patterns that could potentially be ascribed to certain variations in the EVA composition. Totally, three cases of such behavior were identified in the present study for three different groups of BS.

The first case was found for PV modules with non-fluoropolymer BS composed of rutile titania (R) pigment-filled PET air side, pure PET core, and inner R-filled polyethylene (PE) layer. This group of modules was designated as "PET" according to the air-side polymer (Table 1). Totally, 24 field-aged 60-cell PET-type modules were tested by UVF imaging and R_{iso} measurements. The modules were produced in 2012–2013 by the same

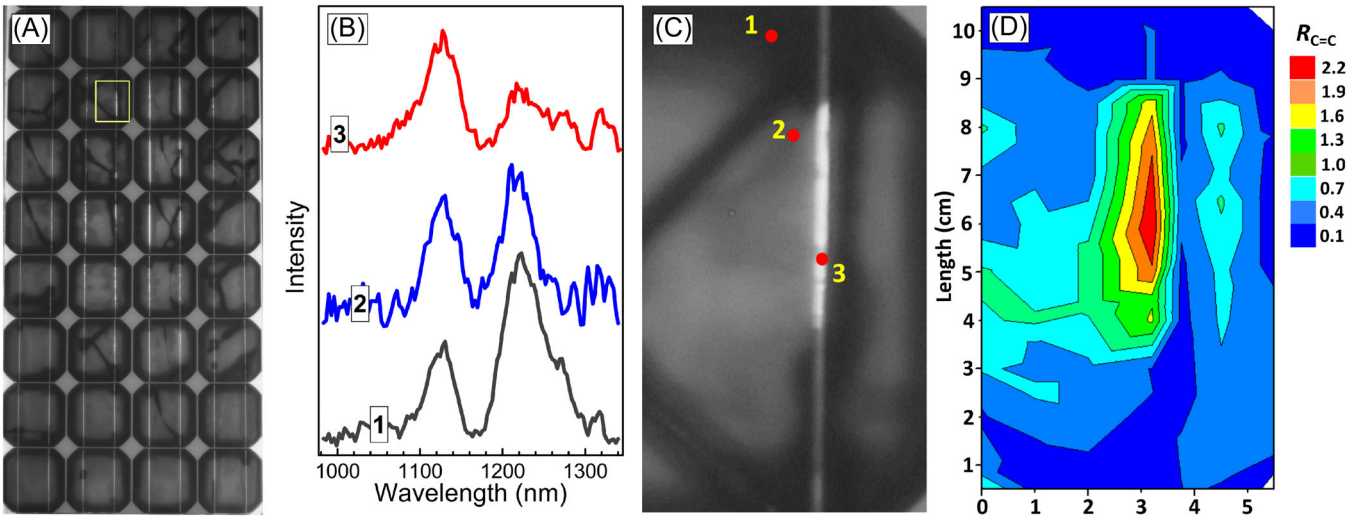

FIGURE 1 (A, C) UV-excited fluorescence image of a module used for near-infrared absorption (NIRA) mapping ((A) mapped area marked by a yellow rectangle) and the mapped section (C) with three exemplary spots of NIRA spectra acquisition marked by numbers; (B) second-overtone NIRA spectra recorded on three different spots over the fluorescent EVA layer of a PV module; (D) NIRA map showing the distribution of $R_{C=C}$ over the inspected section of PV module corresponding to the UVF image in (C).

TABLE 1 Summary of the lab-tested PV modules.

Group	Sample identifier	Number of modules	BS structure (thickness, μm)			Carbonyl index (CI)	R_{iso}, MΩ × m^2
			Air	Core	Inner		
PET	PET_{ref}	1	R-PET (60)	PET (150)	R-PE (50)	0.13	2300
	PET1	18				0.18–0.19	200–250
	PET2	6				0.13–0.14	1000–1200
DF	DF_{ref}	1	R-PVF (30-35)	PET (250)	R-PVF (30-35)	0.11	3040
	DF1	18				0.14–0.15	300–500
	DF2	25				0.10–0.11	800–1400
PA	PA_{ref}	1	R-PA (50-60)	R-PA/PP (300)	R-PA (50-60)	0.13	480
	PA1	16				0.14–0.15	300–500
	PA2[a]	5				0.12–0.13	0.3–0.5

[a]Rectangular cracks observed on BS air side corresponding to the gaps between Si cells.

manufacturer and were installed on a solar PV plant in Southern Germany for 8–9 years before being taken for the lab measurements. In addition, a new (not field-aged) PET-type module was used as a reference. The reference module (PET_{ref}; Table 1) differed from the field-aged ones by manufacturer and production year (2020) but features the same BS structure.

The tested modules were found to form two distinct subgroups, designated PET1 and PET2, with different geometry of UVF pattern (Figure 2) and different R_{iso} values (Table 1). In particular, the PET1 group showed rectangularly shaped UVF emission spots over Si cells with relatively broad dark "quenched" areas around the bright rectangles. The PET2 group revealed much narrower quenched rims, while the bright rectangles featuring rounded corners, rims of higher UVF intensity as well as multiple dark spots in the middle of the cells, and quenched areas along the bus bars. The PET2 group was characterized by drastically higher R_{iso} values as compared to PET1 (Table 1).

From both subgroups, random samples were selected for cross-sectional Raman imaging of the BS structure, revealing identical composition and structure of the PET1 and PET2 BS, and, therefore, the differences in UVF patterns and insulation behavior originate most probably from differences in the EVA encapsulant.

3.1.3 | NIRA spectroscopy of EVA encapsulants

High-resolution NIRA spectra of EVA encapsulant in PET1 and PET2 samples (Figure 3A) registered over metal interconnects[17] showed a distinct C=O-related absorption band at 2140 nm, which could be used to evaluate the carbonyl group density in the EVA encapsulant inside the PV module as a ratio of the intensities of a characteristic C=O band (I_{2140}) and the intensity of a reference C–H band at 1730 nm (I_{1730}), further referred to as an EVA carbonyl index (CI) = I_{2140}/I_{1730}.

We note that no EVA fluorescence can be observed over metal interconnects in UVF images of all our tested PV modules, indicating that UVF is strongly quenched in the spots where NIRA measurements were performed. These spots are therefore not representative of the entire modules showing bright UVF patterns over Si cells but rather characterize a lower limit of the EVA oxidation in each particular module.

It was found that PET1 samples reveal distinctly higher CI values as compared to PET2 as well as to the reference module PET_{ref} (Table 1). This finding was further supported by Raman spectroscopic investigation of two selected EVA samples from modules PET1 and PET2. Carbonyls in acetate groups of EVA reveal a characteristic vibration band at 1750 cm^{-1} (Figure 3B).[17] After normalization to a reference C–H band at 1444 cm^{-1} (Figure 3B, insert), the C=O band of the PET1 sample showed distinctly higher intensity than the same band of the PET2 sample. In summary, both NIRA and Raman measurements indicated a higher C=O content in PET1 as compared to PET2. At that, PET1 is stronger degraded than PET2, according to the R_{iso} measurements.

Several factors can be responsible for differences in the carbonyl content in the EVA encapsulant. Different module manufacturers can use EVA copolymers produced at a different ethylene/vinyl acetate ratio and have therefore different acetate content. In the module manufacturing stage, the acetate groups are partially

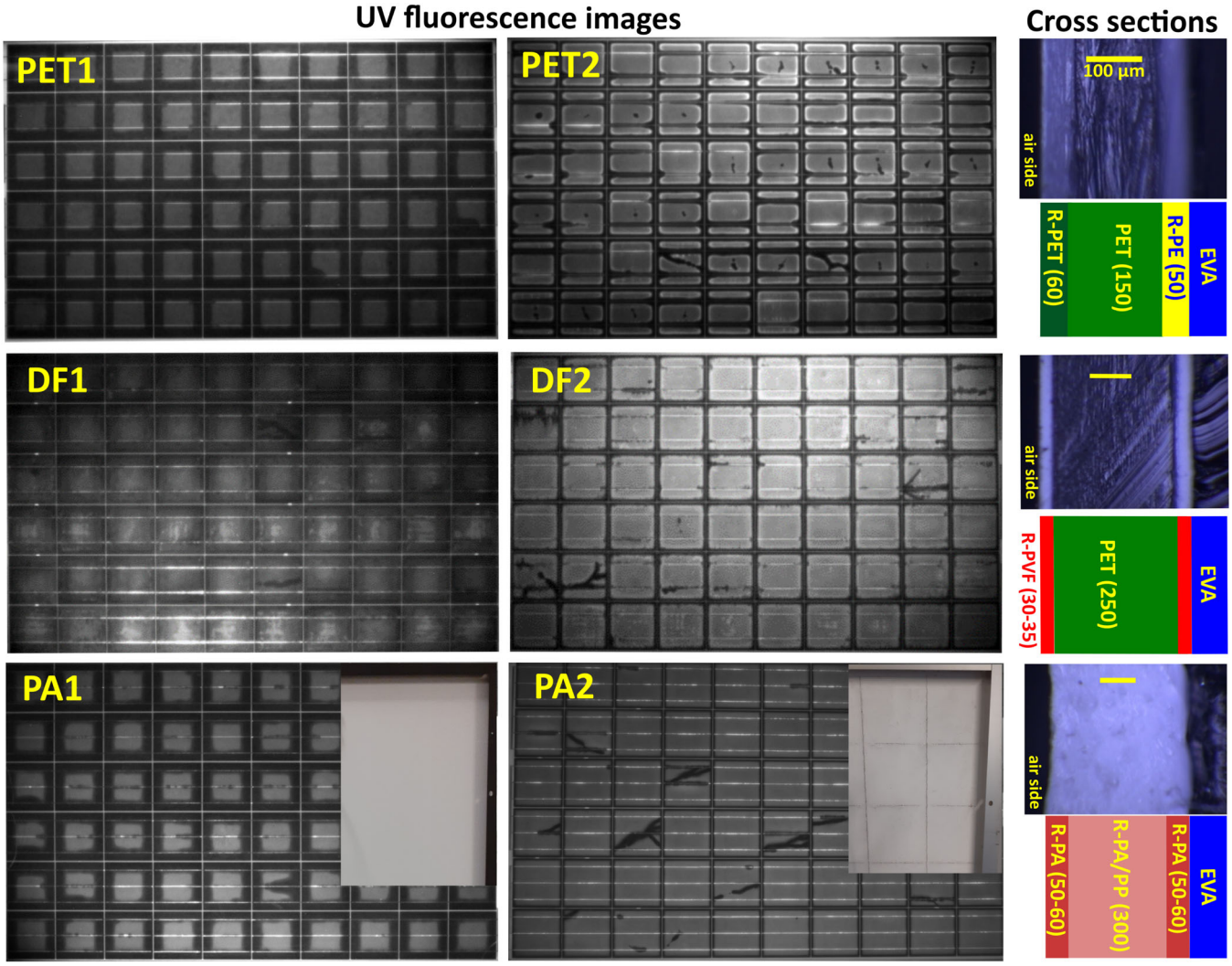

FIGURE 2 UVF images of PV modules with three different BS types (PET, DF, and PA, see Table 1) and cross-sectional structures of corresponding BSs.

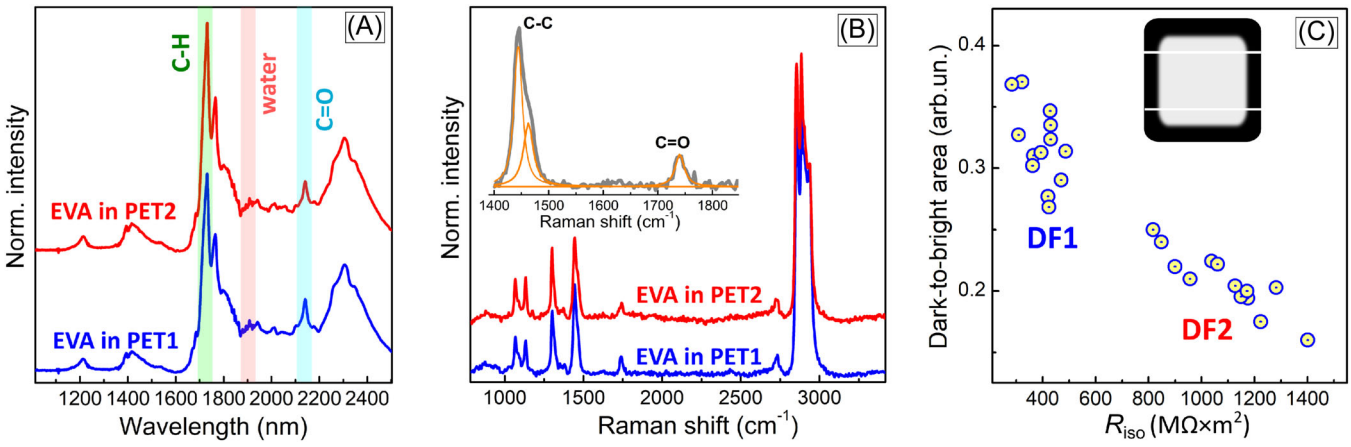

FIGURE 3 (A, B) Normalized NIRA (A) and Raman spectra (B) of EVA samples from PET1 and PET2 modules. Insert in (B) showed an enlarged section of the Raman spectrum of EVA from a PET1 module (gray line) deconvoluted into components by multi-Lorentzian fit (orange lines). (C) R_{iso} of DF-type modules versus a ratio of quenched and emissive EVA areas.

eliminated during the cross-linkage process, which, depending on the conditions and depth of the cross-linking, can result in different CI values for unaged modules.[4,5,21,22] During the field exposure, the EVA encapsulant is subjected to a complex of thermal and photochemical events, including secondary cross-linking as well as photoinduced elimination of acetic acid and formation of C=C species in EVA layers.[20–22]

The BSs are partially penetrable for environmental gases, including air oxygen and moisture, and their insulation capacity depends on the BS composition.[13,15,24] The BS insulation barrier gradually decreases due to degradation induced by environmental factors, and acetic acid evolved as a result of EVA degradation.[16,23,24] Continuous penetration of air oxygen through the BSs can result in the oxidation of C=C species in EVA, resulting in the UVF quenching and formation of additional carbonyl groups.

In summary, the CI in the field-aged modules is a complex function of the BOM, manufacturing conditions, as well as the age and conditions of field exposure. Despite this complexity, for the PV modules with a prolonged field exposure, generally higher CI values are expected for deeper oxidation of the encapsulant. Thus, CI can be used as a parameter characterizing the degradation status of the field-aged modules, which can be measured quickly and nondestructively in the field.

3.1.4 | Effect of EVA encapsulant on UVF patterns—The case of DF BSs

The second case of EVA-dependent UVF geometry was found for PV modules with double-fluoropolymer (DF) BSs. In this case, 43 field-aged 60-cell modules manufactured in 2012 and commissioned on a PV plant in Southern Germany were tested by a combination of UVF imaging and R_{iso} measurements, again showing two distinct groups with different UVF patterns (Figure 2) and insulation resistance, designated as DF1 and DF2 (Table 1).

Similar to the case of PET modules, the DF1 samples show strongly quenched UVF with broad dark rims in the UVF patterns, while the DF2 samples exhibit much brighter rectangular UVF patterns with narrow quenched rims around the bright emission rectangles. Also, the DF1 samples show much lower R_{iso} values as compared to DF2. The multi-spectral Raman imaging of two random DF1 and DF2 samples showed that both have the same BS type (Figure 2; Table 1), and the differences in the UVF and insulation resistance behavior should be expected to come from the EVA component of the modules. In line with this expectation, the DF1 samples showed distinctly higher CI values as compared to DF2 and to the intact reference module DF_{ref}, when tested by NIRA (Table 1) and by Raman spectroscopy (data not shown).

Moreover, we explored a relationship between the UVF intensity and R_{iso} values for 43 modules of the DF group. At that, a ratio of the geometric area of dark (oxidatively quenched) and bright emissive spots of UVF images (see a scheme inset in Figure 3C) was used as a measure of the depth of UVF quenching. We found that lower R_{iso} values correspond to higher dark-to-bright-area ratios (Figure 3C), clearly indicating that deeper UVF quenching indicates a larger loss in insulation resistance. In this way, the geometry of UVF images can be used to evaluate the degradation and insulation state of PV modules.

We note also that Raman measurements of selected BS samples, as well as NIRA measurements of all tested modules, showed no significant differences in the degradation state between PET1/PET2 and DF1/DF2 BSs. In particular, within each group, the BSs showed similar intensity of fluorescence background in Raman spectra and a similar intensity of water-related band in NIRA spectra, both signs indicative of similar degradation status of the tested BS samples.[8,17,18] For this reason, possible differences in the degradation depth of BSs can be ruled out as a significant reason for different UVF pattern geometry of PET1/PET2 and DF1/DF2 modules.

3.1.5 | Effect of EVA encapsulant on UVF patterns—The case of PA BSs

Finally, the third case of EVA-dependent UVF patterns was found for PV modules with non-fluorinated polyamide BSs (PA group, Table 1). This group was composed of 21 field-aged 60-cell modules manufactured in 2011 and commissioned on a PV plant in Eastern Germany. Two distinctly different types of UVF patterns were observed for these modules, allocating them to two different subgroups, PA1 and PA2, the cross-sectional Raman imaging showing them to have identical BSs (Figure 2; Table 1). Unlike the PET- and DF-group modules, both PA subgroups revealed quite a bright EVA fluorescence but with strongly different patterns: PA1 showed rectangular spots in the cell centers with broad quenched areas on the cell periphery, while the PA2 revealed a more homogeneous distribution of UVF intensity above the Si cells with thin quenched rims.

Remarkably, PA1 and PA2 groups showed a different character of field degradation of the BS layer. For the PA1 group, neither mechanical damage of BS nor cracks along the hidden bus bars were observed. At the same

time, the PA2 group showed strong mechanical damage to the BSs with a regular web of rectangular cracks observed between the Si cells, that is, in sections/gaps where solar light can penetrate the entire polymer stack of the module. The PA2 modules subjected to an insulation resistance test showed almost zero resistance (Table 1), most probably indicating that the mechanical damage is not limited by the BS layer but also occurs in both layers of the encapsulant, resulting in a total loss of insulation resistance.

The CI values of PA1 and PA2 are quite close and similar to that of the intact reference PA_{ref} module (Table 1). The variation of CI between PA1 and PA2 is very modest as compared to the CI variation in the PET and DF groups and cannot explain such drastic differences in the geometry of UVF patterns, the character of BS damage, and insulation behavior. Considering the rectangular pattern of BS cracks in PA2 modules that coincide with the gaps between the Si cells, one can safely assume that the BS damage originates from the photochemical degradation of polymers by UV light present in solar irradiation.[14] From this, we can conclude that the EVA encapsulant in such modules does not contain any UV protector additives. A similar decisive effect of additives in the EVA encapsulant for the formation of specific rectangular crack patterns in PA BS was reported by Eder et al.[26]

Dedicated spectral measurements were performed to probe the feasibility of identifying the presence of a UV protector additive in an EVA material of known composition. For this, two commercially available EVA samples were compared, one containing ca. 0.3 wt% of a benzophenone derivative as a UV protector and another without such a UV-blocking additive. The samples were characterized by NIRA, Raman, and UV fluorescence spectroscopies showing identical spectral properties and no noticeable differences for both materials. Therefore, the spectral methods applied in the present work are not sensitive enough to detect such small additives in the EVA encapsulants, even before their cross-linkage processing and field aging. For this reason, the conclusion about the presence/absence of a UV blocker in the field-aged modules with unknown BOM can be done mostly by secondary signs of BS degradation, such as rectangular cracks in PA BSs, indicating an effect of UV irradiation whenever it can penetrate the stack of polymer components of the PV module.

We note that the above-discussed limitation of vibrational spectroscopies in characterizing the presence of additives in the EVA encapsulants refers to the nondestructive inspection of PV modules. In the case of sacrificial sampling, the EVA fragments cut from the tested modules can be subjected to extraction with appropriate solvents, followed by the concentration build-up via solvent evaporation by a factor of 10-100. After the concentration procedure, the analysis of the extract by a combination of vibrational spectroscopies (Fourier-transform infrared, NIRA, and Raman) should become feasible and expected to provide ample information on the content, structure, and degradation pathways of the additives.

3.1.6 | Summary of lab characterization

Summarizing the discussion of lab-based measurements, we note that our results illustrate an important role of EVA composition in the fate and degradation dynamics of PV modules. These differences come, most probably, from the presence/absence of various additives introduced into the encapsulant materials to enhance their resistive properties and suppress degradation. The range of additives is broad, including various cross-linking agents remaining unreacted after the manufacturing, UV filters and stabilizers of different natures, antioxidants, adhesion promoters, and so forth.[4–6] The EVA copolymer itself can exhibit variability of properties, in particular, different ratios of ethylene and vinyl acetate fragments, which can strongly affect the permeability and stability of the encapsulant.[4–6,11] Some variability of the manufacturing process can be expected, resulting in differences in the cross-linking degree and rheology of the EVA encapsulant. In addition, the upper and lower layers of EVA frequently have different properties and additives, contributing to the complexity of phenomena observed after the prolonged field aging of the PV modules.

Our present results illustrate the evidence of this strong influence of EVA on the field aging behavior and underline the need for further deeper investigations. The following discussion of field data is intended to exemplify the possible effects of EVA on the aging/degradation behavior of PV modules for a specific case of PET-type BSs.

3.2 | Field-based characterization

3.2.1 | General field characterization of aged PV modules

BS types of field-tested PV modules were identified by nondestructive NIRA-based measurements, as reported in.[7,18] NIRA spectra of PV modules were recorded and compared with the spectra of known BS types in our BS database. In this way, the BSs of all modules were found to be identical and corresponding to the multilayer PET type, as also discussed in the previous section.

UVF imaging of the test field revealed three distinctly different fluorescence patterns for the modules with the

same PET BS type (Figure 4A) in contrast to only two types found in the lab study. The patterns were designated as EVA1, EVA2, and EVA3, with the pattern EVA1 being generally darker (by UVF inspection) than patterns EVA2 and EVA3. The two latter patterns feature a bright central area and a dark rim caused by a partial UVF quenching due to oxygen and moisture ingress. The quenched rim for type EVA3 is much narrower than for types EVA1 and EVA2. Furthermore, internal structures (cell cracks) can be observed in all UVF images as earlier reported.[20] In general, the patterns EVA2 and EVA3 correspond to the UVF patterns observed in the lab for PET1 and PET2 samples, while pattern EVA1 was not observed in the lab tests.

Visual inspection showed signs of corrosion at metal interconnects (Figure 4B) for ca. 20% of the inspected PV modules. Corrosion was observed as dark spots (rims) over (around) the metal interconnects. Typically, the corroded interconnects were observed in the lower part of the modules.

IR imaging revealed that ca. 3.5% of modules showed PID (shunting type, PID-s). Typical IR images of PID-affected PV modules are presented in Figure 4C. Information about the grounding of the PV system is not available. The PID-affected modules show a varied number of brighter cells, typically close to the edges of the modules; PID-affected modules were always found at the negative end of a string. The occurrence of PID is comparably low, while typically 25%–30% of the PV modules are affected in other tested locations.

3.2.2 | NIRA spectroscopy of EVA encapsulant in the field

NIRA spectra of EVA encapsulant were collected from the front side over metal interconnects. A typical NIRA spectrum of EVA encapsulant reveals several characteristic features (Figure 3A). As discussed in the previous section, the carbonyl band at 2140 nm can be used to evaluate the EVA CI as an intensity ratio of C=O NIRA band at 2140 nm and noncharacteristic C–H band at 1730 nm.

Simultaneously with CI, the *water content in EVA* can be estimated from the same NIRA spectra as an intensity ratio of a water-related band at 1910 nm to the reference band at 1730 nm. We found that water content correlates directly with the EVA CI with a high Pearson correlation coefficient of $R = 0.93$ (Figure 5A). This trend reflects both a faster penetration of water into deeper degraded modules and a higher affinity of deeper oxidized EVA to water molecules. In general, the more oxidized (degraded) EVA contains more water and both parameters can be used to characterize the general degradation status of the PV module.

Finally, the relative reflectivity of metal interconnects can be evaluated from the originally measured NIRR spectra of the EVA encapsulant. As EVA encapsulant has zero absorbance at 1600 nm (Figure 3A), the NIRR spectrum of EVA shows pure reflectance from the metal interconnect at this wavelength. After normalization to the reference NIRR signal at 1730 nm, the reflectivity in arb. un. can be calculated and used as *a measure of the corrosion* of the metal interconnect because the corrosive processes result in light-scattering deposits on the interconnect surface and decrease the specular reflectivity. It was found that the reflectivity of metal interconnects decreases proportionally to an increase in the water content in the EVA encapsulant with a Pearson correlation coefficient of $R = -0.77$ (Figure 5B).

This correlation can be expected if we assume that the major contribution to the metal interconnects corrosion comes from aerobic oxidative processes in a humid environment. Alternatively, the metal degradation can be assumed to occur via anaerobic processes[2,3]

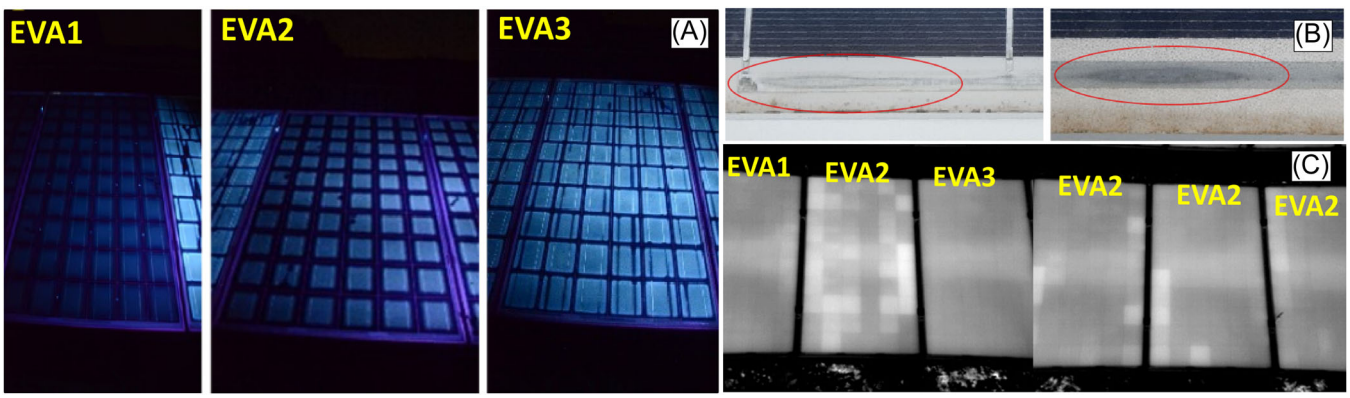

FIGURE 4 (A) UVF images of PV-module samples EVA1, EVA2, and EVA3. (B) Corrosion at metal interconnects for PV-modules EVA1. (C) IR images of PV modules at the string end with EVA2 samples showing PID.

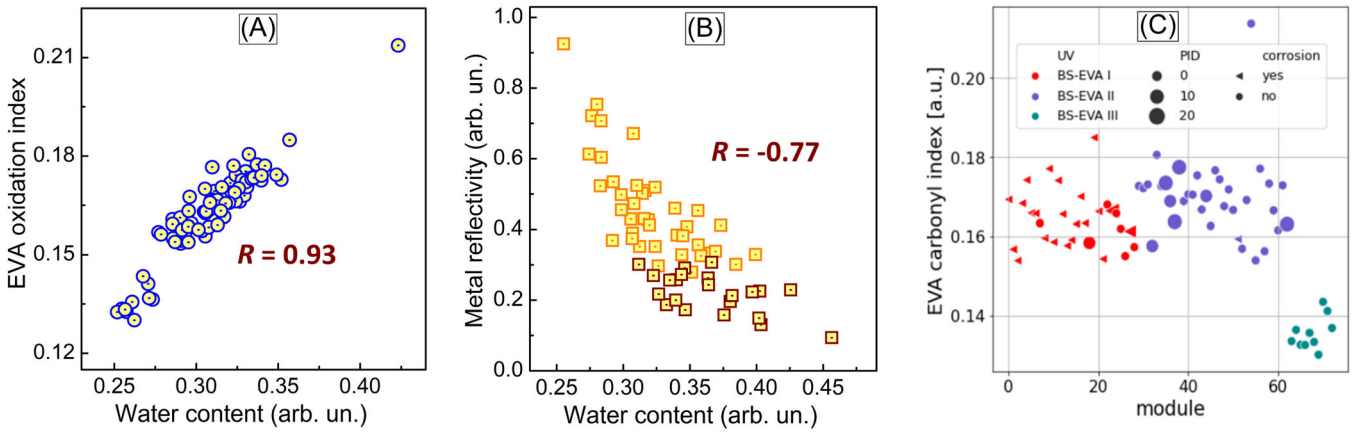

FIGURE 5 (A) Water content in EVA as a function of the EVA CI. (B) The reflectivity of metal interconnects as a function of the water content in EVA; darker squares indicate the modules with visible signs of metal interconnect corrosion; *R* is Pearson's correlation coefficient; darker brown squares represent PV modules with visually observed corrosion signs; (C) CI distribution for different module types, including EVA1, EVA2, EVA3, as well as indicating corrosion-affected and PID-affected modules (by enlarged symbols) sorted by EVA-type. Triangles indicate PV modules with visual corrosion signs.

without the direct participation of moisture, for example, by acetic acid evolved from EVA during the photo-induced degradation of the encapsulant in the field. In this case, a larger amount of evolved acetic acid is expected to result in stronger metal degradation but, at the same time, also in stronger degradation of BS materials, resulting in a loss of insulation resistance and larger penetration of water into the PV module during the field exposure. In both mechanisms, water content is expected to be proportional both to the metal degradation depth and to the degradation state of the polymer insulation of the module, the water acting as a spectrally observable indicator of the general degradation status of the tested module.

3.2.3 | Relations between corrosion, CI of EVA encapsulant, PID occurrence, and UVF geometry

The occurrence of visually discernible signs of corrosion is presented by darker brown squares in Figure 5B as compared to the modules with no appreciable signs of corrosion (lighter orange squares in Figure 5B). It is evident that modules with advanced state of corrosion that can be observed visually correspond to the lower margin of the observed reflectivity range and tend to cluster at higher values of water content. These observations show that the reflectivity of metal interconnects derived from the NIRR spectra of EVA encapsulant can indeed be used to evaluate the corrosion status even for cases where the corrosion signs still cannot be identified by a visual inspection.

For a set of 78 modules, the EVA CI was associated with UVF pattern type by assigning the values to one of three types—EVA1, EVA2, or EVA3 (Figure 5C). It was found that the EVA CI values tend to cluster with respect to the UVF pattern type. The CI variance for the identified UV pattern types was evaluated by Student's *t*-test for independence and found to be statistically significant on a 5% level. The PV modules with EVA1-type encapsulant showed CI values in the range of 0.17–0.20, while EVA2 and EVA3 were found to be less oxidized with CIs at 0.13–0.15. The higher oxidation of EVA1 is in agreement with a very low UVF intensity (Figure 4A), indicating massive oxidative quenching of the EVA fluorescence.

Next, the statistical significance of the observations related to corrosion and PID was evaluated by a chi-square test of independence suitable for nominal data. The test confirmed that the occurrence of PID is statistically significant for EVA2-type modules and corrosion for EVA1-type modules. Modules with high CIs show either PID or corrosion; for modules with low CI (EVA2 type) no signs of degradation were found yet. Thus, corrosion of metal interconnects for EVA1 type modules is associated with high EVA CIs deduced from the NIRA spectra, a comparatively low EVA fluorescence intensity, as well as with the NIRR spectral data. PID of EVA2-type modules is related to high EVA CIs and high EVA fluorescence intensity. But PID is only formed if the modules of EVA2 type are positioned at the string end. CI values of modules with corrosion (EVA1-type) or signs of PID (EVA2-type) are both high but do not differ statistically. Therefore, the type of degradation (corrosion or PID) cannot be deduced from CIs.

The presented dataset reveals that PV modules with the same BS material vary in degradation depending on the properties of the EVA encapsulant material. We assume that the amount and nature of additives, for example, UV-protecting species, in the EVA layers can differ considerably, resulting in strong differences in UVF images. As discussed in the previous section, we were unable to directly identify the presence of the UV-blocking agents or other additives in EVA by IR spectroscopies and spectral UVF measurements. In view of this, we concluded on the presence of additives by secondary signs, in particular, characteristic damage of BS and/or UVF pattern shape and intensity.

3.2.4 | Summary of field observations

In summary, the set of experimental techniques used for the field inspection in the present work does not allow to draw general and accurate enough conclusions on the presence and character of additives in EVA encapsulants of field-aged PV modules with unknown BOM. At the same time, each of the applied approaches provides some useful "hints" as well as direct and indirect evidence allowing a system of well-grounded assumptions on the properties and composition of EVA to be built. In particular, NIRA spectroscopy allows the BS type and water content as a degradation marker to be identified and exclude possible variation in the BS composition and degradation status as major reasons for observed differences in UVF patterns. A visual inspection of BS reveals characteristic crack patterns in the BS, as for the case of rectangularly cracked lab-tested PA2 samples, and enables preliminary conclusions on the presence/absence of UV-blocking additives in the EVA encapsulant.

The similarities in the UVF patterns of the lab-tested PA2 modules and field-tested EVA3 samples observed despite different BS types allow us to assume that EVA3 also has no UV-blocking additives in the EVA layers. At the same time, the UVF patterns of EVA2 and EVA3 are very close to the UVF patterns of the lab-tested PET1 and PET2 samples which show a different CI. In contrast to EVA1, both EVA2 and EVA3 show no considerable signs of corrosion and a high UVF intensity.

Based on these facts, EVA2 and EVA3 can be assumed to contain additives preventing deep degradation of the EVA layer and retaining relatively high UVF. The EVA2 samples reveal a lower UVF intensity and broader quenched rims in UVF patterns, indicating a deeper oxidative degradation of the encapsulant. The EVA1 samples most probably do not contain any UV-blocking additives and have the lowest UVF intensity. These modules are, therefore, most affected by the degradative processes, showing a generally lower reflectivity of the metal interconnects and abundant visual signs of corrosion.

Figure 6 shows a schematic workflow for the differentiation of EVA types using the present methodology. As the first step, we identify the BS type by applying NIRA spectroscopy. Then, we observe different UVF patterns for the same BS type, indicating the presence of EVA encapsulant with a different BOM, in particular, with different sets of additives.

A visual inspection of BSs is performed simultaneously with the analysis of UVF patterns. The presence of characteristic features, such as rectangular cracks in the BS, as in the case of lab-tested PA2 samples, indicates the absence of UV-blocking additives in the EVA encapsulant. In this way, two sorts of EVA with different BOMs can be recognized for the same BS type.

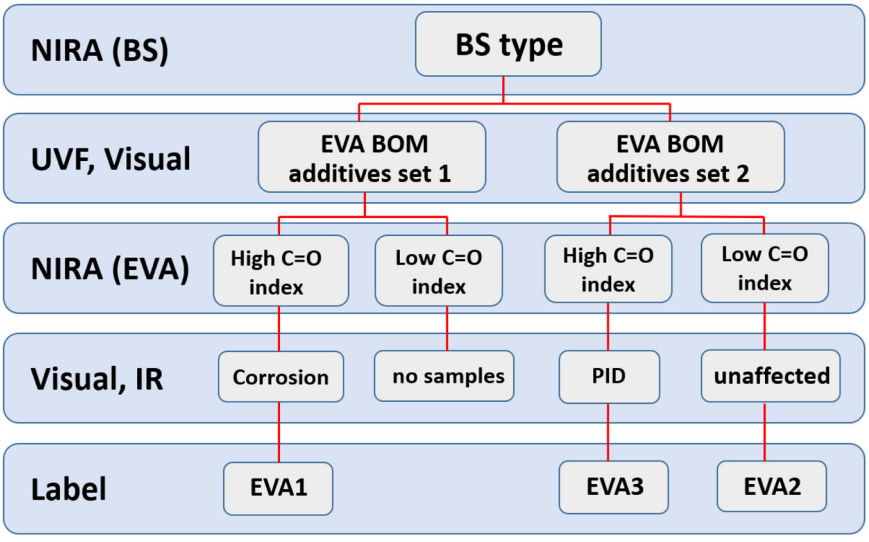

FIGURE 6 Schematic workflow for the differentiation between different EVA materials by a combination of spectroscopic and imaging methods.

The following NIRA inspection of the frontal EVA layer allows for discrimination of field-aged EVA encapsulants with a different depth of oxidation expressed as different carbonyl indices. Finally, a visual inspection of metal interconnects together with aerial IR imaging of the modules allow specific degradation patterns (metal corrosion, PID, etc.) to be assigned to a certain type of EVA encapsulant and the depth of EVA oxidation.

4 | CONCLUSION

A combination of lab and field observations shows that the depth and the pathway of BS-related PV module degradation depend on a combination of the BOM and the properties of polymers, in particular, BS and EVA encapsulant. Insulation resistance and UVF pattern of a PV module, both of which are indicative of the extent of corrosion, depend on the BS type, differing for non-fluorinated BSs, such as PA or PET, and for fluorinated multilayer BSs. On the other hand, PV modules with identical BSs show different insulation resistances, UVF pattern geometries, and general degradation pictures, which most probably originate from differences in the composition and manufacturing conditions of the EVA encapsulants.

The field-aged modules with identical PET BSs were found to feature various oxidation states of the EVA encapsulants, correlating with insulation resistance and the intensity and geometry of UVF patterns. The differences in the EVA carbonyl indices were assumed to originate from differences in the composition of EVA copolymer (ratio of ethylene and vinyl acetate components) as well as different combinations of additives, including UV filters and antioxidants. Deeper field oxidation of EVA encapsulants was found to translate into lower insulation resistances of field-aged modules. This insulation loss is assumed to stem both from the primary photochemical EVA degradation induced by solar illumination and the secondary oxidative EVA degradation by air oxygen and moisture. Our lab tests showed a clear positive correlation between the carbonyl content in the EVA encapsulant and the insulation resistance of corresponding PV modules.

The presence of UV-blocking agents can strongly affect the temporal evolution of EVA encapsulant degradation, but cannot be detected by the applied spectroscopic methods directly. In the absence of such additives, the PV modules are subjected to a deeper primary photochemical degradation which then results in a faster and deeper secondary degradation of both BS and EVA by penetrating environmental gases (O_2 and moisture). Moreover, the inner layers of BS are exposed to UV fraction of solar irradiation in the absence of UV blockers, opening an additional pathway for the BS degradation, often with clear visual evidence, such as rectangular cracking of the BSs between the Si cells, where UV light can affect the exposed BS, resulting in a total loss of the insulation resistance.

Possible variations in the EVA composition, including variations of vinyl acetate content and the number and composition of additives, result in a broad variety of potential degradation pathways and outcomes, even for the same BS type. This variability becomes even broader and more complicated due to the fact that different EVA materials are applied as upper and lower encapsulation layers. Here, we provide a field-identified example of such variety for PV modules with PET-based BSs which show at least three different types of UVF patterns, indicating three different sorts of EVA encapsulants.

Field measurements indicate direct relationships between the EVA carbonyl indices, water content, and reflectivity of the metal interconnect, the latter characterizing the general corrosion state of the modules. We also tracked specific degradation events, for example, visual signs of severe metal corrosion and the occurrence of PID to specific UVF patterns.

By combining lab and field data, we assigned differences in the module degradation status and EVA fluorescence patterns to several possible combinations of the oxidation depth and the presence/absence of UV-blocking species in the EVA encapsulant. Our assignments of differences in the module degradation status and EVA UVF patterns to specific features of the EVA encapsulant, for example, the presence/absence of UV-blocking additives, are rather tentative. Additional experimental verification is needed to get deeper insights into the contribution of EVA additives to specific degradation pathways. At the same time, the present report conveys a clear message on the complex character of the influence of polymer components on the degradation behavior of PV modules and stimulates further studies in this direction.

ACKNOWLEDGMENTS

This work is supported by the German Federal Ministry for Economic Affairs and Energy (project "COSIMA," FKZ: 0324291A and "dig4morE," FKZ: 03EE1090B), The Bavarian State Government (project "PV-Tera—Reliable and cost-efficient photovoltaic power generation on the Terawatt scale," No. 44-6521a/20/5), and Zentrales Innovationprogramm Mittelstand (ZIM, project "PolymerCHECK," No. 16KN083038). Open Access funding enabled and organized by Projekt DEAL.

ORCID

Oleksandr Stroyuk http://orcid.org/0000-0001-5054-2746

Ian Marius Peters http://orcid.org/0000-0002-1725-0909

REFERENCES

1. Hernández-Callejo L, Gallardo-Saavedra S, Alonso-Gómez V. A review of photovoltaic systems: design, operation and maintenance. *Sol Energy*. 2019;188:426-440.
2. Kim J, Rabelo M, Padi SP, Yousuf H, Cho EC, Yi J. A review of the degradation of photovoltaic modules for life expectancy. *Energies*. 2021;14:4278.
3. Denz J, Hepp J, Buerhop C, et al. Defects and performance of Si PV modules in the field—an analysis. *Energy Environ Sci*. 2022;15:2180-2199.
4. Czanderna AW, Pern FJ. Encapsulation of PV modules using ethylene vinyl acetate copolymer as a pottant: a critical review. *Sol Energy Mater Sol Cells*. 1996;43:101-181.
5. Oliveira MCC, Diniz Cardoso ASA, Viana MM, Lins VFC. The causes and effects of degradation of encapsulant ethylene vinyl acetate copolymer (EVA) in crystalline silicon photovoltaic modules: a review. *Renew Sustain Energy Rev*. 2018;81:2299-2317.
6. Omazic A, Oreski G, Halwachs M, et al. Relation between degradation of polymeric components in crystalline silicon PV module and climatic conditions: a literature review. *Sol Energy Mater Sol Cells*. 2019;192:123-133.
7. Buerhop-Lutz C, Stroyuk O, Pickel T, Winkler T, Hauch J, Peters IM. PV modules and their backsheets—a case study of a Multi-MW PV power station. *Sol Energy Mater Sol Cells*. 2021;231:111295.
8. Buerhop C, Stroyuk O, Zöcklein J, Pickel T, Hauch J, Peters IM. Wet leakage resistance development of modules with various backsheet types. *Prog Photovolt Res Appl*. 2021;30:938-947. doi:10.1002/pip.3481
9. Buerhop-Lutz C, Pickel T, Stroyuk O, Hauch J, Peters IM. Insulation resistance in relation to distribution of backsheet types in strings and inverters. *Sol Energy Mater Sol Cells*. 2022;246:111913. doi:10.1016/j.solmat.2022.111913
10. Buerhop C, Stroyuk O, Pickel T, Hauch J, Peters IM. Evolution of inverter ground impedances for PV-modules with various backsheet types. *Prog Photovolt Res Appl*. 2022. doi:10.1002/pip.3621
11. Thornton P, Moffitt SL, Schelhas LT, Dauskardt RH. Dependence of adhesion on degradation mechanisms of ethylene co-vinyl acetate encapsulants over the lifetime of photovoltaic modules. *Sol Energy Mater Sol Cells*. 2022;244:111818.
12. Kontges M, Morlier A, Eder G, Fleis E, Kubicek B, Lin J. Review: Ultraviolet fluorescence as assessment tool for photovoltaic modules. *IEEE J Photovolt*. 2020;10:616-633.
13. Oreski G, Mihaljevic A, Voronko Y, Eder GC. Acetic acid permeation through photovoltaic backsheets: influence of the composition on the permeation rate. *Polym Test*. 2017;60:374-380.
14. Rånby B. Basic reactions in the photodegradation of some important polymers. *J Macromol Sci A*. 1993;30:583-594.
15. Yuen PY, Moffitt SL, Novoa FD, Schelhas LT, Dauskardt RH. Tearing and reliability of photovoltaic module backsheets. *Prog Photovolt Res Appl*. 2019;27:693-705.
16. Peike C, Hülsmann P, Blüml M, Schmid P, Weiß K-A, Köhl M. Impact of permeation properties and Backsheet-Encapsulant interactions on the reliability of PV modules. *Int Sch Res Notices*. 2012;2012:459731.
17. Stroyuk O, Buerhop-Lutz C, Vetter A, Hauch J, Brabec CJ. Nondestructive characterization of polymeric components of silicon solar modules by near-infrared absorption spectroscopy (NIRA). *Sol Energy Mater Sol Cells*. 2020;216:110702.
18. Stroyuk O, Buerhop-Lutz C, Vetter A, et al. Distinguishing between different types of multi-layered PET-based backsheets of PV modules with near-infrared spectroscopy. *Prog Photovolt Res Appl*. 2022;30(8):859-868. doi:10.1002/pip.3465
19. Stroyuk O, Buerhop-Lutz C, Hauch J, Peters IP. Identification of backsheet type of silicon PV modules from encapsulant fluorescence images. *ACS Appl Mater Interfaces*. 2023;6:4.
20. Pern FJ. Luminescence and absorption characterization of ethylene-vinyl acetate encapsulant for PV modules before and after weathering degradation. *Polym Degrad Stab*. 1993;41:125-139.
21. Schlothauer JC, Ralaiarisoa RM, Morlier A, Köntges M, Röder B. Determination of the cross-linking degree of commercial ethylene-vinyl-acetate polymer by luminescence spectroscopy. *J Polym Res*. 2014;21:457.
22. Schlothauer JC, Grabmayer K, Wallner GM, Röder B. Correlation of spatially resolved photoluminescence and viscoelastic mechanical properties of encapsulating EVA in differently aged PV modules. *Prog Photovolt Res Appl*. 2016;24:855-870.
23. Schlothauer JC, Grabmayer K, Hintersteiner I, Wallner GM, Röder B. Non-destructive 2D-luminescence detection of EVA in aged PV modules: correlation to calorimetric properties, additive distribution and a clue to aging parameters. *Sol Energy Mater Sol Cells*. 2017;159:307-317.
24. Hülsmann P, Weiß KA, Köhl M. Temperature-dependent water vapour and oxygen permeation through different polymeric materials used in photovoltaic-modules. *Prog Photovolt Res Appl*. 2014;22:415-421.
25. Morlier A, Siebert M, Kunze I, Mathiak G, Kontges M. Detecting photovoltaic module failures in the field during daytime with ultraviolet fluorescence module inspection. *IEEE J Photovolt*. 2017;7:1710-1716.
26. Eder GC, Voronko Y, Oreski G, et al. Error analysis of aged modules with cracked polyamide backsheets. *Sol Energy Mater Sol Cells*. 2019;203:110194.

How to cite this article: Buerhop C, Pickel T, Stroyuk O, Hauch J, Peters IM. An insight into a combined effect of backsheet and EVA encapsulant on field degradation of PV modules. *Energy Sci Eng*. 2023;11:4168-4180. doi:10.1002/ese3.1572